http://dx.doi.org/10.21577/0103-5053.20190255

J. Braz. Chem. Soc., Vol. 31, No. 2, 211-229, 2020
Printed in Brazil - ©2020 Sociedade Brasileira de Química

Review

An Overview of the Photocatalytic H_2 Evolution by Semiconductor-Based Materials for Nonspecialists

Ivo F. Teixeira,[a] *Jhon Quiroz,*[b,c] *Mauricio S. Homsi*[b] *and Pedro H. C. Camargo*[c]

[a]*Departamento de Química, Universidade Federal de São Carlos (UFSCar), 13565-905 São Carlos-SP, Brazil*

[b]*Departamento de Química Fundamental, Instituto de Química, Universidade de São Paulo, 05508-000 São Paulo-SP, Brazil*

[c]*Department of Chemistry, University of Helsinki, A.I. Virtasen Aukio 1, 00014 Helsinki, Finland*

The solar-to-chemical energy conversion is promising to tackle sustainability challenges toward a global future. The production of H_2 from sunlight represents an attractive alternative to the use of carboniferous fossil fuels to meet our energy demands. In this context, the water splitting reaction photocatalyzed by semiconductors that can be excited under visible or near-infrared light excitation represents an attractive route to the clean generation of H_2. In this review, we present an overview of the most important concepts behind the H_2 generation, from water splitting, promoted by semiconductor-based systems for readers that were recently introduced to the water splitting topic. Then, we present the main classes of photocatalysts based on semiconductors. For each class of semiconductors, we focused on the examples that lead to the highest activities towards the H_2 production and discuss the operation principles, advantages, performances, limitations, and challenges. We cover metal oxides, sulfides, and nitrides. We also discuss strategies in which these materials are combined, including hybridization with metal nanoparticles, other semiconductors, and carbon dots, to achieve improved performances and circumvent the limitations of the individual counterparts.

Keywords: photochemistry, nanomaterials, composite and nanocomposite materials

1. Introduction

1.1. Energy demand and the hydrogen economy

Developing and utilizing a safe, clean, and renewable energy resource represents the greatest technological challenge facing our global future.[1,2] Due to the rising standard of living and human progress, a dramatic increase in the global energy consumption over the next half-century is expected.[1] The current proven reserves of coal, oil, and gas suggest that this energy need can be, at least partially, met with conventional sources.[3] However, the adverse environmental problems caused by the intensive consumption of fossil fuels have led to an increased interest in the use of alternative, clean energy sources to serve and deliver power to human activities.[2,4,5] Hydrogen (H_2), when produced from appropriate and sustainable starting materials, presents itself as a potential alternative to carboniferous fossil fuels (it has a great energy density, 120-142 MJ kg^{-1}). In this context, the generation of H_2 from water as a starting material and sunlight as an energy input, as opposed to the production from petroleum-based fuels, is of paramount importance. With this in mind, the harvesting of sunlight to drive the water splitting reaction photocatalyzed by semiconductors has emerged as one of the most promising approaches for the sustainable generation of H_2.[6]

1.2. The water splitting reaction

Solar energy and water have an unique and enormous potential as clean, abundant, and renewable resources.[7] In fact, the harvesting and conversion of solar into chemical energy (stored in H_2) by the photolysis of water has become one of the most studied topics in the past decade. The H_2 production by water splitting was first reported

*e-mail: ivo@ufscar.br; pedro.camargo@helsinki.fi

in 1972 by Fujishima and Honda[8] using TiO_2 in a photoelectrochemical cell. Interestingly, the photocatalytic water splitting by semiconductor based technologies has stood out as one of the most promising approaches to solving the world energy crisis.[9] Even though a lot of progress has been achieved in the development of semiconductor photocatalysts, most robust systems still require solar energy input in the ultra-violet (UV) region (e.g., TiO_2) for band gap excitation.[10-14] In fact, over the past 40 years, many of the reported photocatalytic systems exhibited high activities towards the water splitting reaction, producing a stoichiometric mixture of H_2 and O_2 (2:1 molar ratio) under UV excitation with impressive quantum yields. One example is the $NiO/NaTaO_3$:La material, which enabled a 56% quantum yield at 270 nm excitation.[9,15]

While several of the usually employed oxide photocatalysts are only active in the UV region, solar light is composed of ultraviolet, visible and infrared components (accounting for 5, 43, and 52%, respectively), as shown in Figure 1. This means that most photocatalysts that are only active in the UV region suffer from low solar-energy utilization.[17] Consequently, it is still very challenging to design and obtain photocatalysts that are abundant, stable, facile to produce, and that show high quantum yields and performances under visible and/or near-infrared light excitation.[12]

According to the thermodynamics requirements, the conduction band potential should be more negative than the reduction potential of H_2O (0 V *vs*. normal hydrogen electrode (NHE)) for the H_2 generation, and the valence band potential should be more positive than the oxidation potential of H_2O (1.23 V *vs*. NHE) for O_2 generation. Therefore, the band gap energy (E_g) of the photocatalyst should be higher than 1.23 eV (lower than 1000 nm) to enable the water splitting. However, in order to use visible light, it should be lower than 3.0 eV (higher than 400 nm).[15] Despite the band energy requirements, other factors are also decisive to the success of the water splitting reaction in semiconductor photocatalysts. These include charge separation efficiency (avoiding the negative-electron/positive-hole (e^-/h^+) recombination), mobility of the charge carriers (charge transfer), and the lifetime of photogenerated electrons and holes.[18]

The U.S. Department of Energy (DOE) has concluded that a photocatalyst for the water splitting must have solar-to-hydrogen (STH) efficiency equal or higher than 5% in order to meet the economically viable price of US$ 2-4 *per* kg H_2.[19] Until now, this benchmark has not been achieved by any semiconductor-based system. Therefore, it is imperative to develop semiconductor-based photocatalysts capable of achieving this benchmark by being highly active under visible irradiation and presenting proper band structures, high quantum efficiency, low e^-/h^+ recombination rate, and e^-/h^+ long lifetimes.

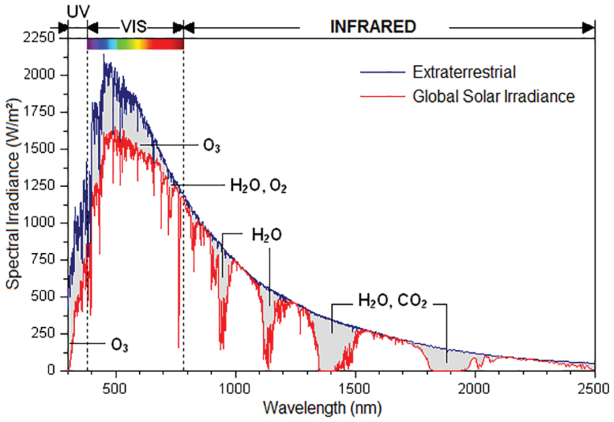

Figure 1. Standard solar spectra as a function of wavelength, displaying the UV, visible and infrared region at the top of the atmosphere and in the ground (adapted from reference 16).

1.3. What do we need to know to perform the water splitting reaction?

The two commonly used experimental set ups employed to perform and measure the water splitting reaction are schematically represented in Figure 2. The main difference among them is the light source irradiation position: being internal (left panel) or external (right panel) relative to the reaction mixture. The internal irradiation reactors, in general, give higher gas evolution rates as the photocatalyst suspension is in closer contact to the light source and thus irradiation of the reaction mixture is more efficient. However, external irradiation reactor is more adequate to mesure quantum yields because of the irregular light-intensity distribution and irradiation area in the internal irradiation reactors.

Before starting the reaction, these systems should be completely degassed by the application of a vacuum or by a flow of inert gas to avoid the intrusion of ambient air into the reactor during the reaction. This, for example, can lead to incorrect estimation of the quantity of photocatalytically evolved gases.[18] Typically, a gas chromatograph with a thermal conductivity detector (GC-TCD) is used to separate, detect and quantify the gases produced during the reaction. Because of this, it is recommended to keep the system online in the GC-TCD. The injection of the gas samples in a separated GC makes the intrusion of ambient gas more likely. Standard gases that represent the gases evolved in the photocatalytic reaction must be used to carefully calibrate the GC-TCD to allow for quantitative analysis.[18]

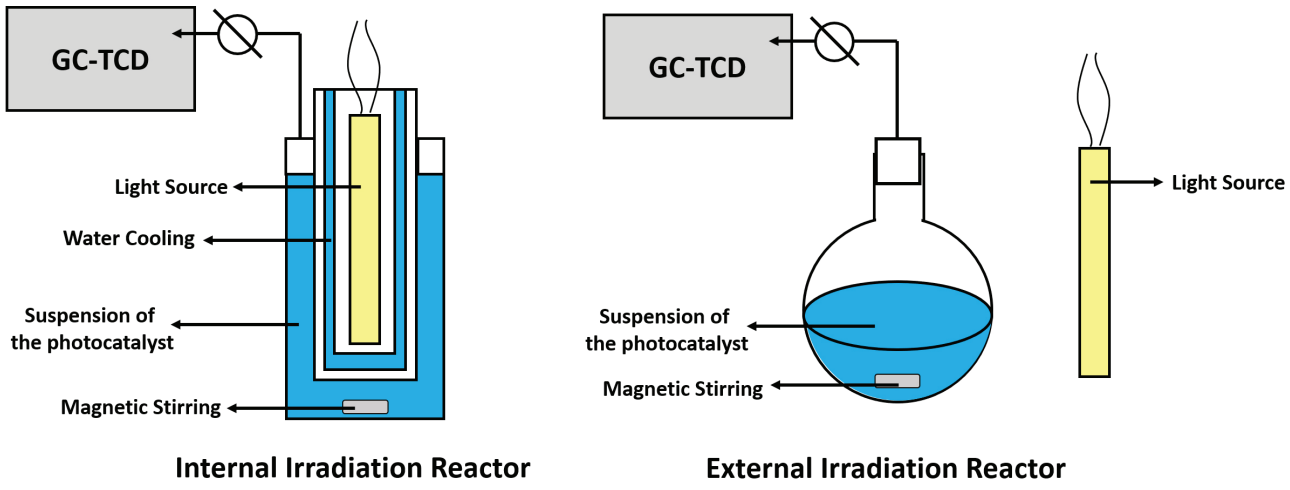

Figure 2. Schematic representation of the commonly used experimental set ups employed to perform the water splitting reaction (adapted from reference 18).

A typical result for the water splitting reaction is schematically represented in Figure 3a. The simultaneous evolution of H_2 (red trace) and O_2 (blue trace) in the expected stoichiometric ratio of 2:1 is shown. Furthermore, a linear increase in the evolved amount of gases with irradiation time is expected.[18]

Sometimes, it is observed the evolution of H_2 and O_2 is not stoichiometric. When H_2 evolved is less than expected stoichiometric amount, this can be an indication of the oxidation of sacrificial reagents and/or self-decomposition of the photocatalyst during irradiation. This is because the quantity of photoexcited electrons consumed in the reduction process must be identical to the amount of photoexcited holes used in the oxidation reaction.[18]

The water splitting reaction photocatalyzed by semiconductor works, at least in principle, in a simple fashion. When a semiconductor is excited by light with energy that surpasses the band gap (energy difference between the valence band and the conduction band), electrons in the valence band of the semiconductor can be excited to the conduction band, while holes are left in the valence band. This creates negative-electron (e^-) and positive-hole (h^+) pairs, also known as exciton.[8,15] This stage is known as the "photoexcited" state. After photoexcitation, as long as the e^-/h^+ recombination is avoided, the excited electrons and holes migrate to the surface of the photocatalyst, acting as reducing and oxidizing agents to produce H_2 and O_2 from H_2O, respectively, as shown in Figure 4.[15]

The performance of semiconductor-based photocatalyst during the water splitting reaction is primarily evaluated based on photocatalytic activity, quantum yield, and STH energy conversion efficiency. Commonly, the photocatalytic activity is expressed as the gas evolution rate normalized by the photocatalyst mass (e.g., mmol g^{-1} h^{-1}). As the evolution rate is highly dependent on the experimental conditions, it is necessary to provide the light source intensity, the reactor type, the irradiation wavelength

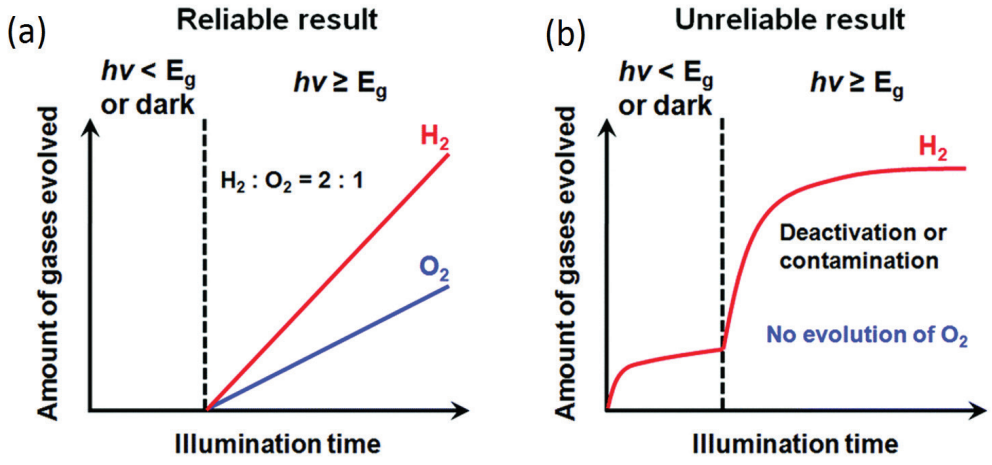

Figure 3. Schematic representation on the evaluation of the photocatalytic activity towards the overall water splitting reaction as a function of the illumination time: reliable (a) and unreliable (b) results (reproduced from reference 18 with copyright permission 2019 from The Royal Society of Chemistry).

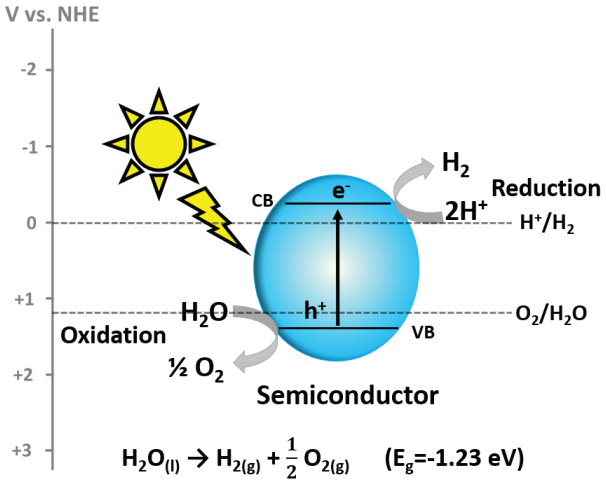

Figure 4. Schematic representation of the water splitting reaction photocatalyzed by a semiconductor. Following light excitation with proper energy, photoexcitation from the valence to the conduction band takes place. The photoexcited electrons and holes participate in oxidation and reduction processes leading to the H_2 and O_2 evolution from H_2O.

range, the reaction temperature, and solution volume. As mentioned, the photocatalytic reaction conditions used by different research groups vary significantly (especially the irradiation conditions). Consequently, direct comparisons of photocatalytic activities may not be helpful. Thus, in order to assess the photocatalyst performance and to be able to compare the obtained results with the present state-of-the-art in the field, the apparent quantum yield (AQY) and STH energy conversion efficiency are more effective datas. The AQY can be calculated using equation 1, where n is the number of e^- or h^+ consumed in the formation of one H_2 or O_2 molecule, R is the quantity in moles of H_2 or O_2 molecules evolved in a specific time interval and I is the number of incident photons reaching the photocatalytic system during the same time interval.[18]

$$AQY = \frac{nR}{I} \quad (1)$$

As the AQY is strongly correlated with the wavelength of incident photons, it is recommended to determine the AQY as a function of irradiation wavelength. More detailed aspects of the photocatalytic activities and AQY measurements can be found in Wang *et al.*[18] and Qureshi and Takanabe[20] works. STH, differently from AQY which uses a concept of photon flux, uses the concept of photon energy. STH is determined by equation 2, where r_{H_2} is the H_2 evolution rate, ΔG_r is the Gibbs energy for the water splitting reaction, P_{sun} is the energy flux of sunlight (100 mW cm^{-2}) and S is the irradiated photocatalyst area.

$$STH = \frac{r_{H_2}\Delta G_r}{P_{sun}S} \quad (2)$$

It is important to highlight that ΔG_r can be used in equation 2 solely for the case that O_2 is generated as the product of H_2O oxidation. Furthermore, the ΔG_r for water splitting is dependent on the reaction pressure and temperature, consequently it has to be adjusted according to the different experimental conditions.[18]

Many excellent reviews regarding the H_2 generation through the water splitting reaction photocatalyzed by semiconductor-based systems have been published.[15,18,21-26] Here, rather than discussing all the different examples and reported photocatalysts, we aim at providing a more focused overview on the main classes of semiconductor-based materials for the water splitting reaction. Specifically, the selected photocatalysts were organized and discussed by their classes and their combinations/modifications that enable one to achieve the best activities and quantum efficiencies that have been reported to date. Our main goal is to present the reader with an updated comparison between the most active photocatalysts that are currently in progress. We believe that this discussion can pave the way and direct readers to the most promising semiconductor-based candidates towards the water splitting reaction and their relative performance comparisons. It is important to clarify that the present review will be solely focused on the photocatalytic water splitting promoted by semiconductor-based catalysts. The photo-eletrochemical approach will not be covered here. Interested readers are referred to recent reviews on this subject.[22,26-29]

2. Types of Photocatalysts

A wide range of semiconducting materials have been developed and employed as photocatalysts towards the H_2 evolution from water. In the subsequent sections, we will focus on the most relevant classes of photocatalytic materials. These will include metal oxides (e.g., TiO_2, Nb_2O_5, WO_3), metal sulfides (e.g., CdS, MoS_2, ZnS), and nitrides (e.g., polymeric carbon nitrides, β-Ge_3N_4). Then, their combination or modifications (to form hybrids and heterojunctions, for example) that lead to higher activities (highest H_2 production rate) and quantum efficiencies will be presented and discussed.

2.1. Metal oxides

TiO_2 was the first reported photocatalyst for the water splitting reaction, producing H_2 and/or O_2 under UV excitation.[30] Colloidal TiO_2, when combined with Pt and RuO_2 nanoparticles as cocatalysts, can generate H_2 with an impressive quantum yield of 30 ± 10% and O_2 in stoichiometric proportions from water under UV excitation

at 310 nm.[31] In this system, Pt and RuO_2 cocatalysts act as electron traps, helping to avoid the recombination of UV-excited electrons and holes and therefore leading to higher photocatalytic activities.

In order to overcome some of the limitations from TiO_2, such as the requirement for UV excitation, other metal oxides have also been studied. These include Nb_2O_5, ZnO, α-Fe_2O_3 and WO_3. Unfortunately, these systems still possess drawbacks.[32,33] For example, ZnO has low photostability as it is easily photo-oxidized under band-gap excitation by photo-generated holes,[32] however, this drawback can be mitigated by using a sacrificial reagent (e.g., S^{2-}/SO_3^{2-}).[34-39] WO_3 is a stable photocatalyst for O_2 evolution under visible light irradiation. Nevertheless, it does not have a satisfactory band structure to allow for the H_2 evolution due to its low-lying conduction band level. α-Fe_2O_3 is not stable under acid conditions, which is a condition used to facilitate the hydrogen evolution.[15] Additionally, it also has a low conduction band level, which is not proper to promote the H_2 evolution.[33] Nb_2O_5 possess a band gap of ca. 3.4 eV and therefore does not absorb in the visible region.[40] Not even the niobate species in their pure form can promote the H_2 evolution under visible light irradiation. Interestingly, niobate catalysts exchanged with H^+, Cr^{3+}, and Fe^{3+} ions present higher activities under UV irradiation than their precursor $K_4Nb_6O_{17}$. It is worth to highlight the H^+-exchanged $K_4Nb_6O_{17}$, which showed the highest activity for H_2 evolution among these niobate species, presenting a quantum yield up to ca. 50% at 330 nm.[41,42]

2.2. Metal chalcogenides

Metal sulfides represent potential candidates as photocatalysts for the H_2 evolution reaction under visible light excitation.[43] They serve as promising alternatives relative to metal oxides. In general, the valence bands of metal sulfides consist mostly of the sulfur 3p orbital. Consequently, their valence band is more negative and has a narrower band-gap compared to metal oxides.[33] Among the several metal sulfides, CdS is one of the most investigated examples due to its suitable band-gap (2.4 eV) and proper band positions for the photocatalyzed water splitting under visible light excitation.[32] However, CdS has frequently been reported[15] to be unstable for photocatalytic H_2 evolution. This is because its S^{2-} anion can be self-oxidized by photoinduced holes in the valence band of the CdS.[15] Such photocorrosion is, in fact, a common problem to most metal sulfide photocatalysts. One of the most used strategies to reduce their photocorrosion is the addition of hole scavengers, including S^{2-} or SO_3^{2-}, in the reaction medium. In this context, CdS in S^{2-}/SO_3^{2-} solution presents a 1017.2 μmol g^{-1} h^{-1} H_2 formation rate. Moreover, its activity can be increased 10-folds when 1.7 wt.% of Pt is supported on it as a cocatalyst to suppress electron-hole recombination.[43]

Other metal sulfides that are active towards the water splitting reaction under visible light irradiation include $CuInS_2$ and $AgInS_2$. Both materials can produce H_2 and O_2 in the presence of sacrificial reagents (S^{2-}/SO_3^{2-}) with relatively good stabilities. Despite the fact that $CuInS_2$ and $AgInS_2$ present lower H_2 evolution than CdS, both systems display similar behavior in which its activity can be increased by 10-folds when loaded with Pt as cocatalyst.[44,45] ZnS, similar to TiO_2, requires excitation in the UV region due to its 3.6 eV band-gap. In the presence of S^{2-}/SO_3^{2-}, ZnS can display longer stability and greater H_2 formation (18818.9 μmol g^{-1} h^{-1}) than CdS. Furthermore, its H_2 evolution can be further improved when 1.7 wt.% of Pt is employed as photocatalyst (21769.0 μmol g^{-1} h^{-1}).

Despite the fact that pure MoS_2 does not produce any H_2 photocatalytically, it is also an important metal sulfide for the photocatalytic water splitting reaction. When CdS is loaded with only 0.2 wt.% of Mo_2S, its H_2 evolution rate is increased up to 36-folds. This hybrid photocatalyst and the reason behind its impressive activity will be discussed in more detail in section "3.1. Coupling semiconductors and metal nanoparticles".[32]

2.3. Nitrides

Among several photocatalysts, polymeric carbon nitride (PCN) has emerged as an attractive candidate to perform the water splitting reaction due to its ability to absorb light efficiently in the visible and near-infrared ranges, chemical stability, non-toxicity, straightforward synthesis, and its earth-abundant composition (only C and N). In fact, PCN is the most active metal-free photocatalyst for the H_2 evolution using solar energy.[19,46,47] Despite the fact that PCN presents proper electronic structure and band position for excitation by visible light, it suffers from the high recombination rates of photogenerated electrons and holes. This, in turn, leads to low quantum efficiency (< 0.1%). An efficient strategy commonly used to overcome this high recombination rate is the hybridization of PCN with metal nanoparticles or with another semiconductor to form hybrids.[47] Both strategies will be discussed in more detail in sections "3.1. Coupling semiconductors and metal nanoparticles" and "3.2. Semiconductor combinations".

β-Ge_3N_4 is another example of nitride that is active for the H_2 evolution. Its photocatalytic activity towards the water splitting in its pure form is negligible. However, when RuO_2 nanoparticles are supported on its surface, β-Ge_3N_4

becomes photocatalytically active for the stoichiometric evolution of H_2 and O_2 from water, without requiring any sacrificial reagents. Unfortunately, β-Ge_3N_4 has a band gap of ca. 3.8 eV, which is only active under UV irradiation.[33,48,49]

2.4. Current limitations of oxides, chalcogenides, and nitrides as photocatalysts for the water splitting reaction

The development of a photocatalyst that splits water efficiently under visible and/or near-infrared light irradiation ($\lambda > 400$ nm) is indispensable to maximize solar energy utilization (UV light only accounts for 4% of the total solar energy). Figure 5 presents a schematic diagram of the band structures for the most important photocatalyst towards the water splitting reaction encompassing metal oxides, chalcogenides, and nitrides. Theoretically, the maximum solar to hydrogen (STH) efficiency is only 3.3% when using UV light, even at a 100% quantum yield. This value is, unfortunately, insufficient for practical solar hydrogen production.[18] Until recently, only a few metal chalcogenides and oxides, such as CdS and WO_3,[48,50-53] had been known to be active under visible light. Some metal chalcogenides, including CdS and CdSe, exhibit a band gap sufficiently small to allow absorption of visible light and have conduction and valence bands at potentials that allow for the water reduction and oxidation reactions. However, they are not stable under the water splitting conditions, once the S^{2-} and Se^{2-} anions are more susceptible to oxidation than water, causing the CdS or CdSe catalyst to self-oxidize.[15,54] Although WO_3 is stable and active under visible irradiation for O_2 evolution, its conduction is located at a more positive potential than the potential of water reduction, not allowing the reduction of H^+ into H_2.[48] PCN, on the other hand, presents an excellent band structure and great stability, however, it has a poor quantum efficiency due to its high recombination rate.

Therefore, it can be observed that these classes of photocatalysts have limitations regarding their application towards the water splitting reaction under visible or near-infrared light excitation. In this context, a promising approach for overcoming these drawbacks is the modification of these semiconductors or their combination to form hybrid materials. For example, band-gap engineering has been used to improve their visible light absorption while the combination with metal nanoparticles (NPs) or with other semiconducting materials has been employed to promote charge separation and suppress charge recombination. These strategies will be the focus of the next sections. Specifically, we will discuss the combination of semiconductor photocatalysts with metal nanoparticles (Figure 6a), other semiconductors to form heterojunctions (Figure 6b) or Z-scheme materials (Figure 6c), and carbon materials (such as carbon dots (CDs), Figure 6d) to achieve superior water splitting performances while overcoming the limitations presented by the use of these catalysts (oxides, chalcogenides, and nitrides) in their pristine or individual form.

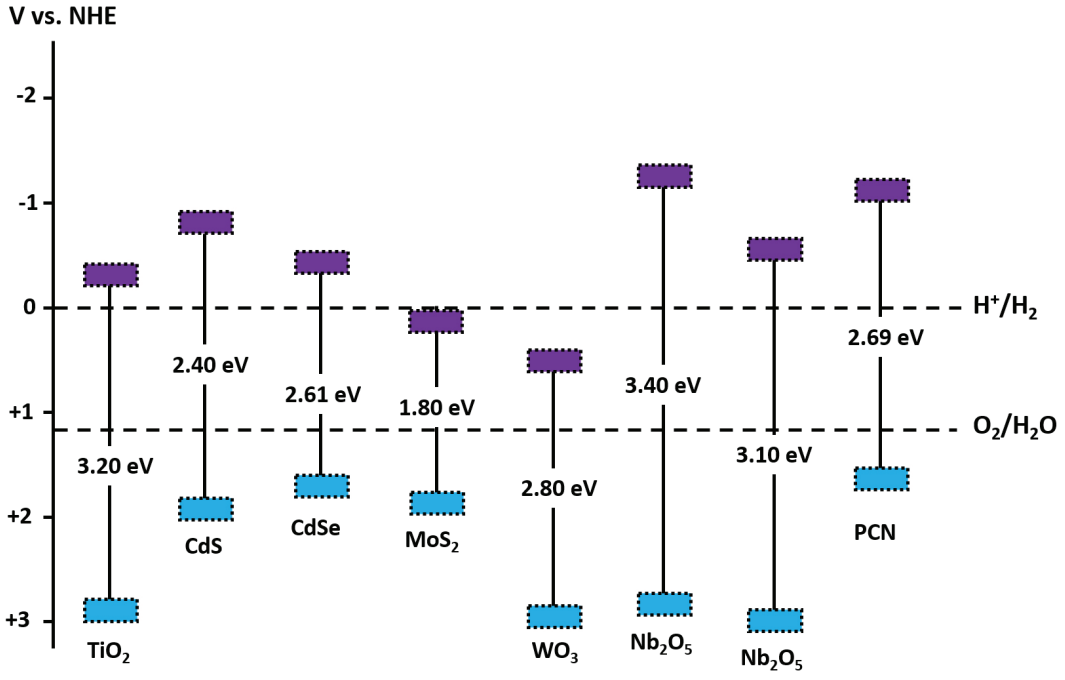

Figure 5. Schematic illustration of the band structures and potentials for various semiconductor photocatalysts (oxides, chalcogenides, and nitrides) employed towards water splitting relative to the water reduction and oxidation reactions.

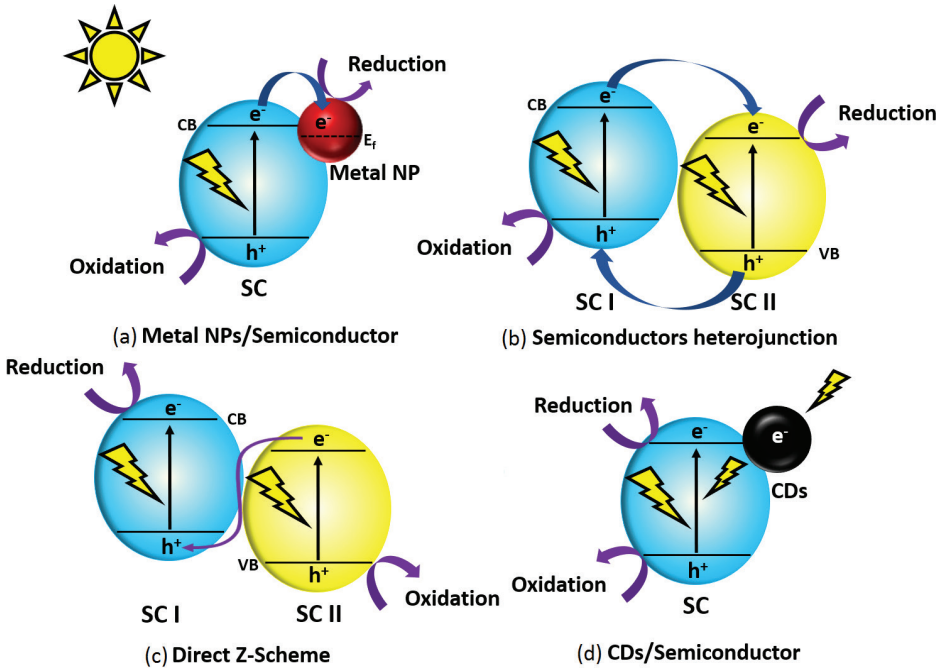

Figure 6. Strategies to improve the photocatalytic performance of semiconductors towards the water splitting reaction by their combination with metal nanoparticles forming Schottky junctions (a), with other semiconductors generating heterojunctions (b) and Z-schemes (c), and with carbon dots (d).

3. Hybrid Semiconductor-Based Photocatalysts

3.1. Coupling semiconductors and metal nanoparticles

One of the most used strategies to promote charge separation and suppress charge recombination is to combine a semiconductor material with a cocatalyst, such as a metal nanoparticle.[55,56] The metal nanoparticles can lead to the formation of junctions (an Ohmic-type or Schottky-type contact) that allow charges to flow in the right direction at the interface between the semiconductor and the cocatalyst.[55,56] It can also provide active sites that promote H^+ reduction and H_2O oxidation by lowering the respective activation energies.[18] Common examples of metal nanoparticles employed as cocatalysts with semiconductors include Ni, Ru, Pt, Pd, Ir and Rh, which, in general, promote the H_2 evolution. On the other hand, Fe, Ni, Mn and Co based oxides tend to favor the O_2 evolution.

Metal nanoparticles, when deposited on a semiconductor surface, generate a contact potential difference due to their different work functions.[57] This potential difference is called the Schottky barrier. As shown in Figure 7, the band bending when a contact is formed after reaching equilibrium is dependent on the relative energies of the work functions of the metal (ϕ_M) and the semiconducting (ϕ_B) components. This phenomenon can greatly enhance the charge separation efficiency, once it can induce the directional migration of photogenerated electrons from the semiconductor to the metal.[58] In other words, it can lead to the generation of effective electron trapping site to suppress the electron-hole recombination. When plasmonic nanoparticles are coupled with semiconductors, they not only act as electron traps, but they also can lead to the generation of localized heating, near-field enhancements, and charge-transfer processes at the interface between the metal and semiconductor.[59]

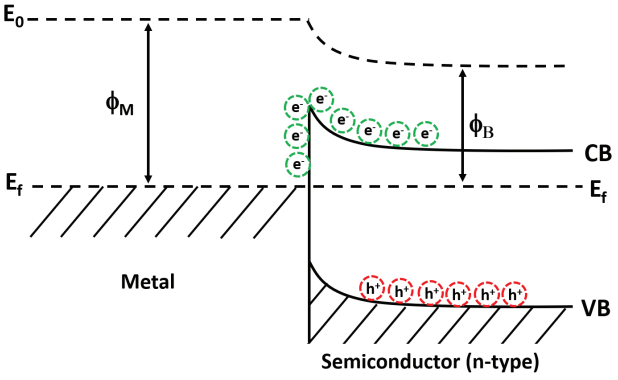

Figure 7. Band structure for a hybrid material composed of a metal (cocatalyst) and a semiconductor (photocatalyst) nanoparticle in contact under equilibrium, when the metal work function (ϕ_M) is higher than the semiconductor work function (ϕ_B) (adapted from reference 57).

One of the classical examples of hybrid materials comprising a semiconductor and a metal nanoparticles that has been applied for the photocatalytic water splitting is Pt/TiO_2.[8,60] Here, Pt acts as electron traps and thus serves as

catalytic centres that favor the H_2 evolution.[8,60] In another example, Haruta and co-workers[61] have reported a study on photoassisted H_2 production from solutions of water/ethanol by Au/TiO_2. In terms of efficiency under similar conditions, Au/TiO_2 presented poorer activity (about 30% less active) relative to Pt/TiO_2. However, the Au based system is more active under visible light excitation due to the localized surface plasmon resonance (LSPR) effect, which represents an important advantage when compared with the Pt/TiO_2.[60,61] The Au NPs introduce visible light photo response in TiO_2 due to the LSPR excitation, which causes injection of LSPR excited hot electrons (electrons with energy above the Fermi level as a result of LSPR excitation) from the Au NPs into the conduction band of TiO_2.[60,61] Primo *et al.*[62] reported enhanced activity for water photooxidation by Au/CeO_2 nanocomposites at wavelengths matching the Au LSPR position (visible light) and in presence of Ag^+ as a sacrificial electron acceptor. In this system, CeO_2 (without supported Au nanoparticles) showed negligible activity under visible irradiation. The authors justified the catalyst activity under visible-irradiation thanks to the same phenomena which occurs with Au/TiO_2 (electron injection into semiconductors conduction band).[62]

Another semiconductor that has been decorated with metal nanoparticles for the improvement of performances towards the photocatalytic water splitting is the polymeric carbon nitride (PCN). As this semiconductor is already active under visible light excitation, it is less dependent on the use of sensitizers to enable absorption in the visible range and thus increase the water splitting performances. Because of this, one of the most studied nanoparticles in combination with PCN is Pt. Interestingly, Pt has been studied in conjunction with PCN in a variety of forms, ranging from nanoparticles to single-atoms.[63-74] For example, Li *et al.*[68] investigated single-atom Pt as a cocatalyst in PCN for the H_2 evolution. They reported that single-atom Pt as cocatalysts led to tremendous enhancements on photocatalytic H_2 generation, being 8.6-folds higher than that of Pt NPs (*per* Pt atom basis), and nearly 50-folds higher relative to bare PCN.[68]

It is important to mention that PCN is a relatively complex and versatile structure, in which its performance can be further optimized by tuning its structure via controlled synthesis. For example, Tang and co-workers[70] were capable to improve the activity of a PCN (synthesised from urea; containing 3 wt.% of Pt; employing triethanolamine (TEOA) as a hole scavenger) via controlled synthesis to achieve record values under visible irradiation (> 395 nm). They reported an H_2 evolution rate of 19412 μmol g^{-1} h^{-1} with a quantum yield of 26.5% (at 400 nm excitation).[70] Rhodium (Rh) was also demonstrated to increase photocatalytic H_2 production activity of PCN when it is used as cocatalyst under visible light illumination.[75] Other non-noble metals were also successfully used supported on PCN to enhance H_2 evolution, such as Ni, Cu, Zn, Co, and Fe.[76-79] Despite it increment the PCN activity, so far, they have not been as active as noble metals as cocatalysts.

Although PCN is active under visible light excitation, its hybridization with plasmonic metals such as Ag and Au also represent efficient strategies to further enhance their performances towards the H_2 evolution as a result of LSPR excitation, not only by injecting electrons on PCN conduction band, but also promoting charge transfer from light-excited PCN.[80,81] For instance, Guo *et al.*[82] reported that the controlled synthesis of Au/PCN can lead to excellent activities to H_2 evolution. Their optimized 18 nm-sized Au nanospheres/PCN photocatalyst exhibits a rate of 540 μmol g^{-1} h^{-1} under visible light ($\lambda > 420$ nm).[68,82]

In addition to the plasmonic NPs, hybrids containing three different components have also shown great promise. Hybrid materials comprised of Ag NPs combined with carbon dots (CDs) and PCN were 6.7 folds more active towards the H_2 evolution relative to bare PCN and 2.8 folds higher than CDs/PCN.[47] This synergistic effect is due to the combination of LSPR effect from Ag NPs with upconverted photoluminescence (PL) superiority of CDs, which allowed for a broader spectrum applications.[47] Coupling CDs with semiconductor photocatalysts as photosensitizers or cocatalysts is becoming a quite common strategy to improve semiconductor-based systems activity in photocatalysis.

Another efficient strategy to enhance semiconductors activity towards the photocatalytic H_2 evolution is the utilization of bimetallic systems to create hybrid materials. Various bimetallic cocatalyst systems have been developed. Among them, it is important to highlight Rh/Cr_2O_3 core-shell NPs and PdAg NPs. In Rh/Cr_2O_3, the chromium oxide species have an important role in kinetically preventing that the evolved O_2 reaches the metal surface, thereby limiting the undesirable water formation reaction.[18,83] Interestingly, PdAg supported on PCN presented an impressive rate of H_2 evolution under solar irradiation (1250 μmol g^{-1} h^{-1}) with great stability. Furthermore, this system also shows an excellent quantum efficiency (8.7%) compared with other visible active systems.[84] The authors[84] attributed this enhancement to the inherent property of Pd metal to quench photogenerated electrons by the Schottky barrier formation mechanism and strong visible light absorption due to the characteristic surface plasmon resonance (LSPR) of Ag NPs along with the absorption of PCN (Figure 8).

Despite the hybridization of semiconductors with metal nanoparticles represents an effective strategy to

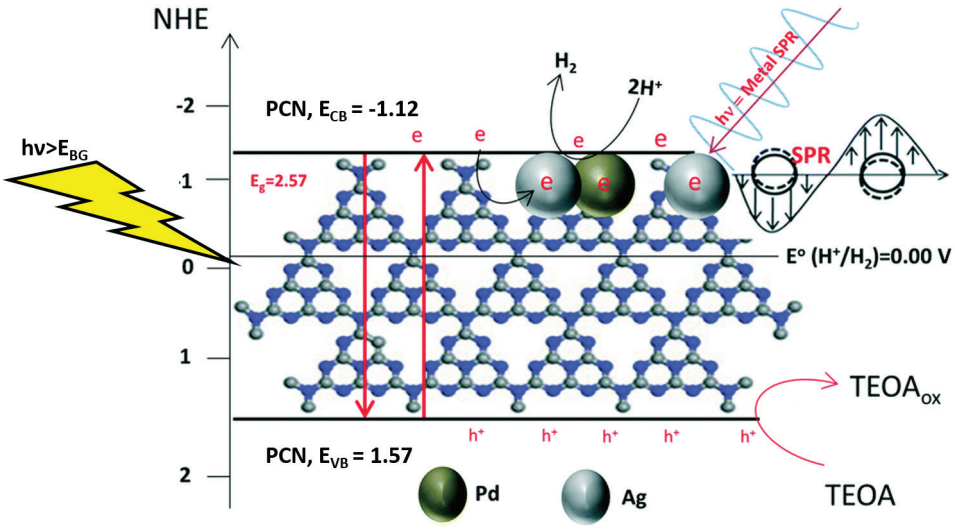

Figure 8. Schematic illustration of the H_2 evolution, charge transfer, and LSPR effect in the $Pd_{0.7}Ag_{0.3}$/PCN under visible light irradiation (reproduced from reference 84 with copyright permission 2018 from The Royal Society of Chemistry).

enhance photocatalytic performances towards the H_2 evolution, several systems still do not present good quantum efficiencies in the visible or near-infrared ranges. Thus, strategies to further improve these systems are needed. One of these strategies is the combination of two or more semiconductors to form heterojunctions or Z-schemes, which will be the focus of the next section.

3.2. Semiconductor combinations

One of the most used semiconductors in photocatalysis is TiO_2, which is not active in the visible range. In order to make TiO_2 active in this region, several combinations between TiO_2 and other semiconductors have been proposed. This particular topic has been comprehensively reviewed by Marschall.[27] Among the TiO_2-based photocatalyst applied in the photocatalytic H_2 evolution, $CuAlO_2/TiO_2$ represents a remarkable example. This material presented an impressive H_2 evolution rate of 21060 μmol g^{-1} h^{-1} under visible irradiation (> 400 nm) and in presence of sacrificial reagent (S^{2-}/SO_3^{2-}).[85] The authors[85] attributed the enhanced photoactivity to the more efficient charge separation enabled by the semiconductor combination. Both the TiO_2 doping and combination with other semiconductors represent classical examples of band-gap engineering to make them active under visible irradiation.

As mentioned in the previous sections, CdS has proper band positions to be active for H_2 evolution under visible light excitation. However, it suffers from poor stability in solution, particle agglomeration, and high recombination rates of photogenerated e^-/h^+ pairs. These issues severely limit its practical application for the photocatalytic water splitting.[25] A common strategy to increase the CdS stability is the use of a hole scavenger compound, as cocatalysts. One example is Ag_2S. In this specific case, Ag_2S captures the h^+ formed in CdS, which is used in the oxidation of sulfite ions (sacrificial reagent), consequently making the CdS less susceptible to self-oxidation.[86]

The hybridization of CdS with MoS_2 also represents an efficient approach to avoid e^-/h^+ recombination in CdS and allow for increased H_2 evolution rates. When loaded with 0.2 wt.% of MoS_2, the H_2 evolution rate for this system (CdS/MoS_2) is increased by up to 36 folds.[87] Even higher activities can be obtained by growing CdS nanocrystals on the surface of a nanosized MoS_2/CdS hybrid. Ye and co-workers[88] reported 1800 μmol g^{-1} h^{-1} of H_2 evolution rate with a quantum efficiency of 28.1% (420 nm) for these systems (S^{2-}/SO_3^{2-} employed as a sacrificial reagent). Despite the good results, the CdS-based systems still suffer from the limitations regarding its long term stability.

Hybrids composed by the combinations of CdS with tungsten carbide (WC) also have shown to improve H_2 evolution. The WC/CdS hybrid photocatalyst exhibited a H_2 evolution rate comparable to that of Pt/CdS under visible light irradiation (S^{2-}/SO_3^{2-} employed as a sacrificial reagent).[89] Interestingly, when Pt metal nanoparticles are loaded on the surface of CdS, WC provides active sites to promote the H^+ reduction, leading to a fast diffusion of photogenerated electrons from CdS towards WC and a more efficient charge separation.[89]

In another example, Xie *et al.*[90] reported mesoporous CdS@ZnS core-shell NPs as active photocatalyst for the H_2 evolution from water (729 μmol g^{-1} h^{-1}). Its activity was explained based on a charge transfer mechanism. Here, under visible light excitation and considering the

band alignments, both the electrons and holes formed in the CdS core cannot transfer to the ZnS shell due to its higher conduction band (CB) and lower valence band (VB) position. However, the authors proposed that the presence of acceptor states within the band-gap allowed the transfer of holes from photoexcited CdS to the ZnS shell as illustrated in Figure 9, which is similar to the mechanism of charge transfer in dye sensitized solar cells (DSSCs). This charge transfer promotes the charge separation and consequently improves the photocatalytic activity.[90]

In terms of quantum efficiency under visible light excitation, CdS-based photocatalysts stand out. Li and co-workers[91] reported a quantum yield of ca. 93% at 420 nm for a CdS photocatalyst loaded with 0.30 wt.% of Pt and 0.13 wt.% of PdS as cocatalysts. Furthermore, this same photocatalyst presented an impressive H_2 evolution rate of 23233 μmol g^{-1} h^{-1} in the presence of sacrificial reagents (S^{2-}/SO_3^{2-}) and under visible-light irradiation.[91] Other examples that deserve to be mentioned in terms of high performances are the nanoporous solid solutions of ZnS-In_2S_3-Ag_2S[92] and ZnS-In_2S_3-CuS.[93] Both systems exhibited an extremelly high visible-light H_2 evolution rate (220000 and 346000 μmol g^{-1} h^{-1}, respectively) from water (S^{2-}/SO_3^{2-} employed as a sacrificial reagent). Furthermore, they also presented excellent quantum yields (19.8 and 22.6% at 420 nm, respectively).[92,93] Despite the impressive results for these two solid solutions photocatalysts, their stability under the reaction conditions were not reported.

Biswal and co-workers[94] reported an N-doped Ga-Zn mixed oxides with hierarchical morphology (loaded with 3 wt.% Rh and 1.5 wt.% Cr_2O_3 as cocatalysts) capable of producing H_2 from a methanol aqueous solution with an apparent quantum efficiency of 5.1% and an H_2 evolution rate of 37202 μmol g^{-1} h^{-1} under visible-light illumination. Despite the high H_2 production rates, this study was not conclusive about the enhancement mechanism behind the activity of the N-doped Ga-Zn/Rh/Cr_2O_3 photocatalyst, especially due to the high complexity of this photocatalytic system.

Regarding PCN based photocatalysts, one of the major limitations is the e^-/h^+ recombination rate. In order to overcome this challenge, many heterojunctions between PCN and other semiconductors have been described. They include CdS/Au/PCN,[95] NiS/Ni/PCN,[96] CdZnS/Au/PCN,[97] $Cd_{0.8}Zn_{0.2}S$/Au/PCN,[98] PCN/Pd/Cu_2O[99] and PCN/Ag/MoS_2.[100] The hybrid systems that present the highest activities, in general, have a Z-scheme architecture and will be discussed in more detail in the next section. However, it is important to highlight the NiS/Ni/PCN heterostructure. This material presents an H_2 evolution rate of 515 μmol g^{-1} h^{-1} (> 420 nm), which is the highest H_2 evolution rate reported for a system that is noble-metal free and does not involve organic sensitizers.[96] It is important to mention that several other semiconductors heterojunctions have been studied toward the photo(electro)catalyzed water splitting reaction. Although these systems were not described herein, the excellent review by Tang and co-workers[25] on this topic is recommended for interested readers.

3.3. Formation of Z-scheme systems

Although the examples discussed in the previous section demonstrate that designing heterostructures is promising to separate electron-hole pairs, the photocatalytic properties of these systems are limited as a result of the weak redox abilities of the generated charge carriers. In

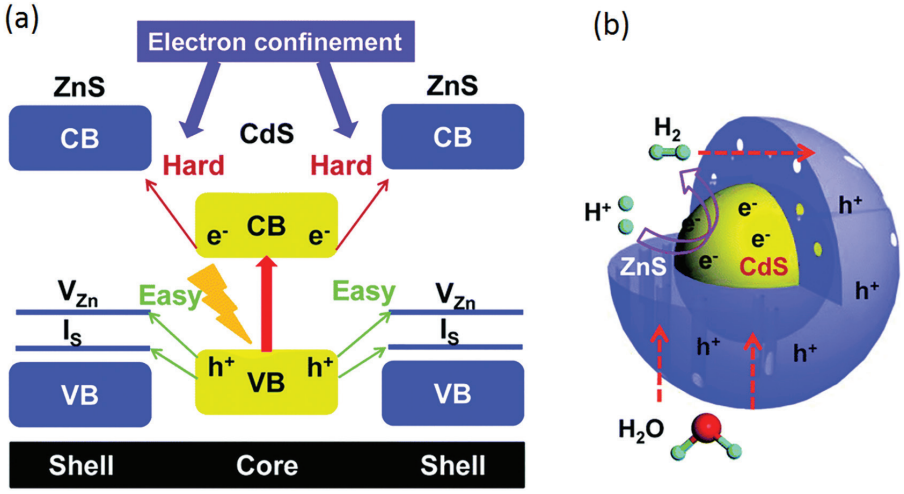

Figure 9. (a) Band structure alignments of the CdS@ZnS core-shell nanoparticles; (b) schematic illustration of the photoexcited charge carrier distribution and the water splitting reaction promoted by CdS@ZnS core-shell nanoparticles (reproduced from reference 90 with copyright permission 2014 from The Royal Society of Chemistry).

this context, the Z-scheme based photocatalysts prepared through the rational integration of two narrow-band-gap semiconductors can pave the way to efficiently separate the photogenerated charge carriers while maintaining strong redox properties and a broader range of solar light harvesting. These features result from the unique structure and charge carrier transfer pathway Z-scheme systems, which is similar to that of a type-II heterojunction photocatalyst, but its charge-carrier migration mechanism is different. In this case, a typical direct Z-scheme system has a charge-carrier migration pathway that resembles the letter "Z" as depicted in Figure 6c. Interested readers can refer to some excellent reviews[18,24,101,102] on this topic for more details regarding principles and mechanism of Z-scheme photocatalysts. Here, we will highlight how Z-scheme systems enable the tailoring photocatalytic performance to drive the water splitting reaction. Specifically, our focus will be devoted to recent achievements in terms of H_2 evolution.

As stated in the previous section, TiO_2 and their corresponding heterojunctions have been widely used to photocatalalyze the H_2 evolution. We can take advantage of the Z-scheme to enhance the photocatalytic activity of TiO_2 by combining with semiconductor materials with suitable band-gaps. Zhang and co-workers[103] have exploited this approach by conducting studies on the coupling of WO_3 with TiO_2 to form a solid-state Z-scheme photocatalytic system towards the H_2 evolution. They produced TiO_2/WO_3 nanofibers via the electrospinning technique. The authors found that the H_2-production rate drastically increases from undetectable for pure TiO_2 to 27.73 μmol g^{-1} h^{-1} in TiO_2/WO_3. They postulated that this higher efficiency is related with the hole collector properties of WO_3 which suppresses the charge recombination process resulting in more photogenerated electrons in TiO_2 available to reduce H^+ to H_2.[103] In other studies,[104,105] the authors focused on TiO_2/WO_3 Z-scheme heterojunctions loaded with metal nanoparticles like Pt and Au. The use of Pt as cocatalysts results in a significant improvement in the H_2 evolution reaction rate, reaching 128.66 μmol g^{-1} h^{-1}. Interestingly, the use of Au illustrates the dependence with the irradiation regime, i.e., UV *vs*. visible illumination. Upon UV light irradiation, Au NPs can serve as an electron sink for conduction band electrons transferred from the TiO_2 in TiO_2/WO_3, thereby enhancing electron-hole pair separation. However, under visible irradiation, the photocatalytic H_2 production rate is dominated by SPR-mediated electron transfer from Au NPs to TiO_2. Herein, the H_2 production was 165.57 and 269.63 μmol g^{-1} h^{-1} under UV and visible light irradiation, respectively.

It is of particular relevance to this discussion Z-scheme systems employing CdS. It has been established that CdS, when loaded with a cocatalyst or coupled with other semiconductors, displays good performance in photocatalytic H_2 production. In this context, an interesting report evidenced how CdS/WO_3 achieves an efficient Z-scheme for hydrogen evolution under visible light.[106] The authors found an optimal CdS loading (20 wt.%) that was able to boost the H_2 evolution rates by more than 5 folds when compared to bare CdS, from 73 to 369 μmol g^{-1} h^{-1}. Further understanding of this system by introducing Pt as cocatalyst was also reported. Interestingly, the authors succeeded to place the Pt nanoparticles between CdS and WO_3, resulting in a $CdS/Pt/WO_3$ heterostructure with a good H_2 generation rate of 2900 μmol g^{-1} h^{-1}, surpassing that of CdS/WO_3 by 7.9 folds under visible light irradiation.[106]

More recently, Guo *et al*.[107] developed an efficient Z-scheme photocatalysts composed of oxygen deficient ZnO_{1-x} nanorods and $Zn_{0.2}Cd_{0.8}S$ nanoparticles (Figure 10). This heterojunction, with an optimal 10 wt.% ZnO_{1-x} loading, exhibited an exceptionally high H_2 generation rate of 2518 μmol g^{-1} h^{-1} with an apparent quantum efficiency of 49.5% at 420 nm excitation. This was 25 folds higher than pure ZnO_{1-x} and 20 folds higher than the $Zn_{0.2}Cd_{0.8}S$ counterpart. The excellent photocatalytic activity was ascribed to an efficient charge carrier separation provided by the Z-scheme together with a visible light absorption enhancement due to the presence of oxygen vacancies in the sample. More recently, the advantages of employing a hierarchical Z-scheme ZnO/CdS system were evidenced by Wang *et al*.[108] The authors found an excellent H_2 reaction rate of 4134 μmol g^{-1} h^{-1} for the sample with optimal CdS content (30.9%) without noble metal cocatalyst.[108] Despite the excellent H_2 reaction rate, the authors used UV irradiation (365 nm) and the photocatalyst presented stability issues, losing about 20% of its efficiency in the first 16 h.

The Z-scheme approach has also been explored to boost the photocatalytic efficiency of polymeric carbon nitride (PCN). Kailasam *et al*.[109] have achieved the Z-scheme mechanism over mesoporous PCN/WO_3 composites prepared by simply dispersing WO_3 powders with mesoporous PCNs. The optimized composite loaded with 3 wt.% of Pt showed a steady evolution of H_2 at very high rates of 326 μmol g^{-1} h^{-1} under visible light irradiation. The authors declared that this value was very high compared not only to PCN/WO_3, but also to other PCN/metal oxide composite materials. This enhanced performance was mainly ascribed to: higher surface area, synergetic effect of PCN and WO_3 components with improved charge separation through a preformed physical interface, and enhanced light absorption of the hybrid materials.

Hou *et al*.[110] took advantage of this PCN/Z-scheme principle and designed a ternary hybrid nanofiber comprised of TiO_2/WO_3/PCN aiming to further improve the separation

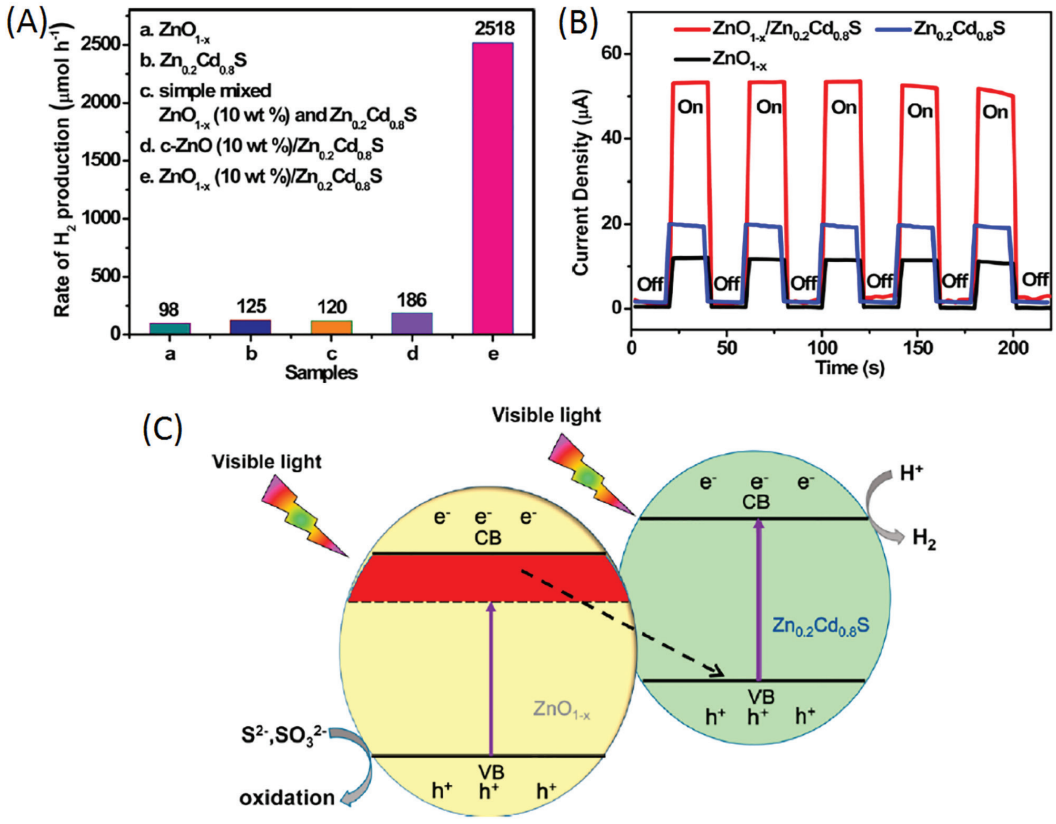

Figure 10. (A) Photocatalytic H_2 evolution rate of different samples under visible-light irradiation ($\lambda > 420$ nm). Reaction conditions: 0.1 g of catalyst in 100 mL aqueous solution containing 0.1 M Na_2S and 0.1 M Na_2SO_3; (B) photocurrent response *vs.* time for $ZnO_{1-x}/Zn_{0.2}Cd_{0.8}S$, ZnO_{1-x}, and $Zn_{0.2}Cd_{0.8}S$ samples ($\lambda \geq 420$ nm) in light on and light off conditions; (C) scheme for the charge separation and photocatalytic H_2n generation process over direct Z-scheme $ZnO_{1-x}/Zn_{0.2}Cd_{0.8}S$ heterojunction (adapted from reference 107).

of the photogenerated carriers while avoiding the use of noble metals as cocatalysts. The nanofiber was obtained by electrospinning followed by a solution dipping process. The resulting ternary nanofiber displayed H_2 evolution rate of ca. 286.6 μmol g^{-1} h^{-1} under visible light irradiation, which is much higher than those obtained for pure TiO_2 (4.3 μmol g^{-1} h^{-1}), pure PCN (77.5 μmol g^{-1} h^{-1}), TiO_2/WO_3 (21.9 μmol g^{-1} h^{-1}), and TiO_2/PCN (169.3 μmol g^{-1} h^{-1}). Herein, the significant enhanced photocatalytic behavior was ascribed to the WO_3/PCN interface developed in the ternary hybrid fibre nanostructure giving rise to the Z-scheme photocatalytic system. Moreover, the authors claim that the robust 1D architecture can not only inhibit the agglomeration of PCN, but also improve the surface adsorption capacity of the reactants.

Defect engineering represents a significant strategy to manipulate the photocatalytic performance of semiconductors since it can increase the spectral response, improve the photogenerated charges separation, promote efficient charge transfer, and contribute towards surface reactions.[111] Very recently, Gao *et al.*[112] reported a dual defective Z-scheme system comprised of defect-rich PCN nanosheets anchored with defect-rich TiO_2 nanoparticles. The optimized photocatalysts showed a superior H_2 evolution rate of 651.79 μmol g^{-1} h^{-1} which presented the highest value when compared to previously reported[31,73] single defective TiO_2 or PCN-based photocatalysts. Moreover, the authors stated that this protocol will provide useful design guidelines for further dual defective PCN/oxides (ZnO, SnO_2, etc.) heterostructures.

The role of reduced graphene oxide (rGO) as an effective solid-state electron mediator has been exploited to enhance the interfacial contact between CdS and PCN in a Z-scheme system.[113] This hybrid photocatalyst comprised of CdS coupled rGO dispersed on exfoliated PCN nanosheets was prepared by hydrothermal approach. A remarkably enhanced H_2 production rate was obtained for the Z-scheme CdS/RGO/PCN composite containing the optimal content of PCN (50 wt.%) (676.5 μmol g^{-1} h^{-1}) with an excellent quantum efficiency (36.5%). The authors[113] claimed that the improved performance was a combination of efficient charge transfer/separation and increased specific surface area.

3.4. Carbon dots

Carbon dots (CDs) have emerged as promising

photocatalysts due to their low cost as well as light-harvesting and electron transfer properties.[114] CDs comprise a nanocrystalline region of sp^2 hybridized graphitic carbon clusters (2-10 nm in diameter) isolated by sp^3 amorphous carbon networks. Several reviews[114-117] have focused on the design and fabrication of carbon dots towards photocatalytic energy conversion. Herein, we will highlight the photocatalytic H_2 production activities of representative CDs photocatalysts following the pattern of the previous sections.

Hybridizing semiconductor photocatalysts with CDs as photosensitizers or cocatalysts is receiving increasing attention. A pioneering work[118] underlines the different role of CDs in CDs/TiO_2-P25 hybrid system. The composites were synthesized via a facile one-step hydrothermal reaction and showed approximately 4-times higher photocatalytic H_2 evolution rates than pure TiO_2. It is noteworthy that the photochemical function of this hybrid system depends on the irradiation regime. Upon UV irradiation, the CDs can serve as electron reservoirs to suppress charge carrier recombination in the P25. However, under visible-light irradiation, the CDs behaved as photosensitizers, transferring photogenerated electrons to the conduction band of the P25 to drive H_2-evolution reactions. Ho and co-workers[119] furthered our understanding of these CDs/TiO_2 photocatalysts by integrating the CDs in the ensembles of TiO_2 nanoparticles and nanowires. The composites were prepared hydrothermally using vitamin C as a carbon resource. The optimized NPs/CD nanocomposite generates H_2 at a rate of 739.0 μmol g^{-1} h^{-1}, which represents 9.7 times higher than pure TiO_2 nanoparticles. Regarding the nanowires, the hybrid nanocomposite produces hydrogen at a rate of 1189.7 μmol g^{-1} h^{-1}, which is 4.2 times higher than that of bare TiO_2 nanowires. Other TiO_2-CDs based photocatalysts evidence how the chemical connection in the composites drives more efficiently the H_2 production.[119,120]

It has been demonstrated that PCN and their combinations are promising candidates for photocatalytic H_2 production. Evidences of coupling CDs with PCN for the enhancement in the photocatalytic performance have been reported.[19,121,122] Very recently, Zhao and co-workers[123] shed light on how rational combination of CDs with PCN leads to enhanced photocatalytic performance in hydrogen evolution, which is depicted in Figure 11. The authors incorporated CDs onto PCN nanotubes obtained by thermal copolymerization between freeze-dried CDs and urea precursor. The resulting materials, with Pt as a cocatalyst, could efficiently produce H_2 under visible light irradiation at a rate of 3538 μmol g^{-1} h^{-1} and a notable quantum yield of 10.94% at 420 nm excitation. Mechanistic insights were obtained by spectroscopic and

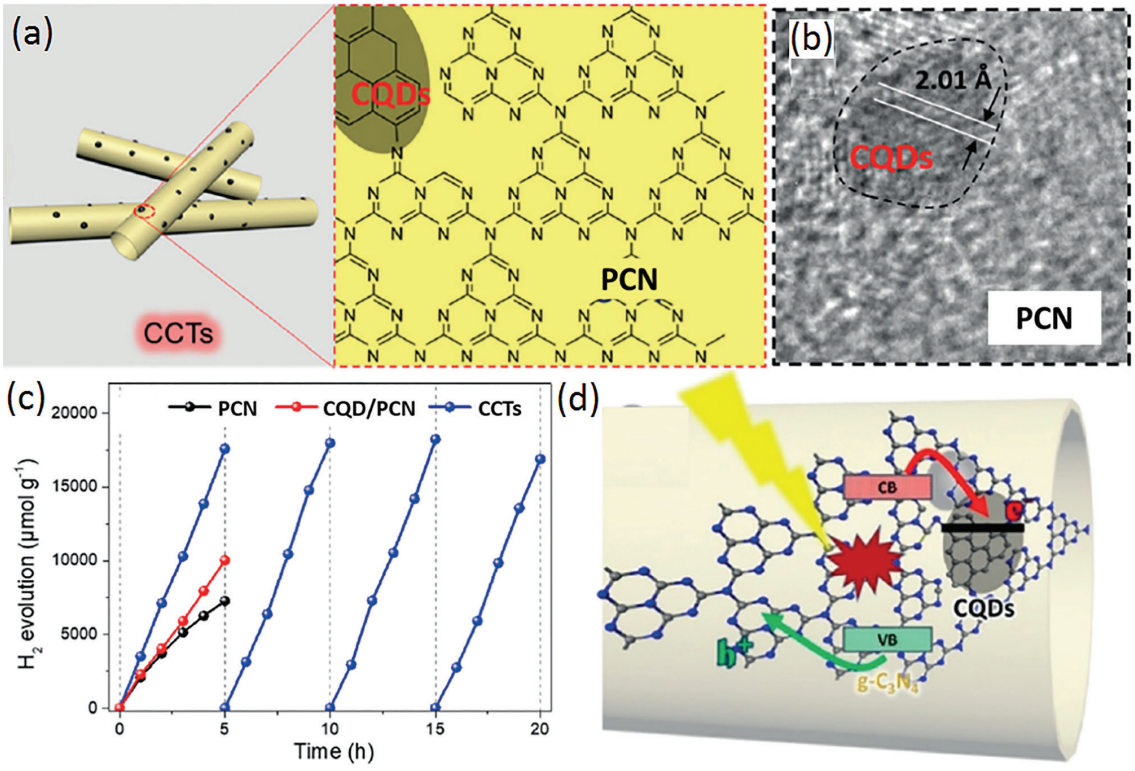

Figure 11. (a) Scheme of the tubular CDs implanted PCN heterostructures (CCTs) via thermal polymerization of freeze-dried urea and CDs precursor; (b) HRTEM image of CCTs highlighting the pattern ascribed to hexagonal crystalline structure of CDs; (c) time course of H_2 evolution experiments for PCN and CCTs under visible light irradiation ($\lambda > 420$ nm); (d) schematic representation of photocarrier separation in CCTs (adapted from reference 123).

photoelectrochemical studies.[123] These studies suggest that the designed structure creates a work function difference between graphite carbon and conduction band of PCN that could spatially promote the charge separation. Interestingly, this CDs/PCN intimate integration also reduces the band-gap increasing the visible light harvesting, thus improving the photocatalytic efficiency for H_2 evolution. These data introduced important parameters to consider for the design of efficient H_2 evolution photocatalysts.

Reisner and co-workers[124] highlighted the use of CDs as light absorber and photosensitizer for a Ni-bis-(diphosphine) molecular photocatalyst for the H_2 production. In this case, the photogenerated electrons from the CDs, that can absorb UV and visible-light, are transferred to the solution containing the molecular Ni catalysts to complete the redox reaction in the system. This hybrid system showed photocatalytic H_2 evolution of 398 μmol g^{-1} h^{-1} and the quantum efficiency was estimated to be as high as 1.4%. Further understanding of this system reveals that CDs graphitization and core nitrogen doping enhanced the photocatalytic H_2 evolution performance.[124] For the hybrid photocatalysts containing graphitized CDs, the H_2 evolution rate was improved almost 7 times when compared to the amorphous CDs. Regarding the molecular catalysts hybridized with core nitrogen doped CDs, they found a significant enhancement in terms of H_2 evolution rates (7950 μmol-H_2 g_{CD}^{-1} h^{-1}) when compared to the graphitized-CDs (1549 μmol-H_2 g_{CD}^{-1} h^{-1}) and the amorphous-CDs (226 μmol-H_2 g_{CD}^{-1} h^{-1}). These observations were attributed to a higher concentration of long-lived photogenerated electrons, as evidenced by spectroscopic measurements. The use of CDs as photosensitisers for solar-driven catalysis has been extensively reviewed by Hutton *et al*.[125]

4. Conclusions and Perspectives

We presented herein an overview of the main photocatalytic systems based on semiconductors towards the water splitting reaction for the production of H_2. For each type of material or material combinations, we discussed their photocatalytic performances, how they work, their advantages, and their current limitations. In particular, rather than discussing the variety of materials that have been employed towards the photocatalytic H_2 evolution from water, we focused on selected examples that have been proven to display the best performances in terms of H_2 evolution rates and quantum efficiencies. Specifically, we started with a discussion on the most important classes of photocatalytic materials, such as metal oxides, chalcogenides, and nitrides. Then, we demonstrated how semiconductor combinations with metal nanoparticles, other semiconductor materials (forming heterojunctions and Z-schemes), and carbon dots can be put to work towards the enhancement of their performances and circumvent the limitation of these materials in their isolated forms. In this case, Table 1 summarizes the main classes of photocatalytic materials that have been described and show the best performances towards the photocatalyzed H_2 evolution.

Table 1. Comparison on the H_2 evolution performance promoted by semiconductor-based photocatalysts

Catalyst	Reactant solution	Light source (wavelength / nm)	Activity / (μmol g^{-1} h^{-1})	QE (wavelength) / % (nm)	Reference
PCN	100 mL of 15 vol% triethanolamine aqueous solution	300 W Xe lamp (> 420)	1300	4.2 (420)	73
PCN	100 mL of 10 vol% triethanolamine aqueous solution	300 W Xe lamp (> 420)	3600	11 (420)	123
GaN	100 mL of water	500 W high pressure Hg lamp	320	3 (420)	83
		Metal NPs/semiconductor			
Fe_2O_3/TiO_2	38 mL of water	460 W Hg arc lamp	9.2	N/A	30
Pd/CdS	90 mL of 0.24 mol L^{-1} Na_2S and 0.35 mol L^{-1} Na_2SO_3 aqueous solution	125 W high pressure Hg lamp	17029	15 (480)	43
$Pt/AgIn_5S_8$	270 mL of 0.35 mol L^{-1} Na_2S and 0.25 mol L^{-1} K_2SO_3 aqueous solution	300 W Xe lamp (> 420)	200	5.3 (411)	44
$Pt/AgInS_2$–ZnS	220 mL of 0.35 mol L^{-1} Na_2S and 0.25 mol L^{-1} K_2SO_3 aqueous solution	300 W Xe lamp (> 420)	340	N/A	45
Pt/PCN	100 mL of 10 vol% triethanolamine aqueous solution	300 W Xe lamp (> 300)	1860	N/A	46
Mg^{2+}/GaN	700 mL of water	450 W high pressure Hg lamp	812	N/A	49
Pt/CdS	400 mL of 0.24 mol L^{-1} Na_2S and 0.35 mol L^{-1} Na_2SO_3 aqueous solution	125 W high pressure Hg lamp	15470	25 (420)	51
Au/TiO_2	120 mL of 5 mol L^{-1} ethanol aqueous solution	500 W high pressure Hg lamp	1035	N/A	60
Pt/TiO_2	120 mL of 5 mol L^{-1} ethanol aqueous solution	500 W high pressure Hg lamp	1540	N/A	60
Pt/PCN	100 mL of 10 vol% TEOA aqueous solution	300 W Xe lamp (> 420)	140	N/A	63

Table 1. Comparison on the H_2 evolution performance promoted by semiconductor-based photocatalysts (cont.)

Catalyst	Reactant solution	Light source (wavelength / nm)	Activity / (μmol g^{-1} h^{-1})	QE (wavelength) / % (nm)	Reference
Metal NPs/semiconductor					
Pt/PCN	5 mL of 10 vol% TEOA aqueous solution	300 W Xe lamp (> 420)	97.5	0.58 (440)	64
Pt/PCN	200 mL of 10 vol% triethanolamine aqueous solution	300 W Xe lamp	14000	N/A	68
Pt/PCN	230 mL of 13 vol% triethanolamine aqueous solution	300 W Xe lamp	3327.5	26.5 (400)	70
PCN/Ti_3C_2/Pt	50 mL of 10 vol% triethanolamine aqueous solution	300 W Xe lamp	5100	3.1 (420)	74
Ag/PCN	40 mL of 33 vol% methanol aqueous solution	100 W halogen lamp	280	N/A	80
Au/PCN	40 mL of 2.5 vol% triethanolamine aqueous solution	300 W Xe lamp (> 420)	550	0.5 (520)	82
Rh/PCN	40 mL of 10 vol% methanol aqueous solution	300 W Xe lamp (> 420)	19	N/A	75
Ni/PCN	50 mL of 10 vol% triethanolamine aqueous solution	300 W Xe lamp (> 420)	110	2.6 (420)	76
Ni@PCN	100 mL of 10 vol% triethanolamine aqueous solution	500 W Xe lamp	180	N/A	77
PgAg/PCN	25 mL of 10 vol% triethanolamine aqueous solution	solar irradiation	1250	8.7	84
NiO/$K_4Nb_6O_{17}$	300 mL of 3 vol% methanol aqueous solution	450 W high pressure Hg lamp	77	3.5 (330)	41
Semiconductor heterojunction					
Ag_2S/CdS	120 mL of 0.25 mol L^{-1} sodium sulfite aqueous solution	150 W solar simulator	850	N/A	86
MoS_2/G-CdS	300 mL of 20 vol% lactic acid aqueous solution	300 W Xe lamp (> 420)	9000	28.1 (420)	88
WC/CdS	100 mL of 0.1 mol L^{-1} sodium sulfide aqueous solution	500 W Hg arc lamp (> 420)	1300	N/A	89
CdS@ZnS	270 mL of 0.1 mol L^{-1} sodium sulfite aqueous solution	300 W Xe lamp (> 400)	800	N/A	90
Pt/PdS/CdS	100 mL of 0.5 mol L^{-1} sodium sulfide aqueous solution	300 W Xe lamp (> 420)	27000	88 (420)	91
$ZnIn_{0.23}Ag_{0.04}S_{1.365}$	320 mL of 0.6 mol L^{-1} sodium sulfide aqueous solution	300 W Xe lamp (> 420)	220000	19.8 (420)	92
$ZnIn_{0.25}Cu_{0.02}S_{1.395}$	320 mL of 1.2 mol L^{-1} sodium sulfide aqueous solution	300 W Xe lamp (> 420)	200000	22.6 (420)	93
NGaZn	20 mL of 10 vol% methanol aqueous solution	125 W medium pressure Hg lamp	37500	N/A	94
CdS/Au/PCN	60 mL of 17 vol% methanol aqueous solution	300 W Xe lamp (> 420)	19	N/A	95
Ni/NiS/PCN	100 mL of 15 vol% triethanolamine aqueous solution	300 W Xe lamp (> 420)	500	N/A	96
NiO/$NaTaO_3$:La	390 mL of water	400 W high pressure Hg lamp	19800	56 (270)	9
Ni/$Rb_4Nb_6O_{17}$	350 mL of water	400 W high pressure Hg lamp	936	N/A	40
Z-scheme heterojunction					
PCN/Au/CdZnS	100 mL of 0.25 mol L^{-1} sodium sulfide aqueous solution	150 W Xe lamp (> 420)	6000	N/A	97
CdZnS/Au/PCN	100 mL of 0.1 mol L^{-1} glucose aqueous solution	300 W Xe lamp (> 420)	123	N/A	98
C_3N_4/Pd/Cu_2O	20 mL of 10 vol% triethanolamine aqueous solution	300 W Xe lamp (> 400)	32.5	0.9 (420)	99
TiO_2/WO_3/Au	70 mL of 35 vol% methanol aqueous solution	300 W Xe lamp	3460	N/A	105
ZnO/CdS	80 mL of 0.25 mol L^{-1} sodium sulfite aqueous solution	350 W Xe lamp	4000	N/A	108
TiO_2/PCN	100 mL of 10 vol% triethanolamine aqueous solution	300 W Xe lamp	66000	4.45 (420)	112
Carbon dots					
CDs/PCN	150 mL of water	300 W Xe lamp (> 420)	575	16 (420)	19
CDs/TiO_2	25 mL of 25 vol% methanol aqueous solution	500 W halogen lamp (> 450)	500	N/A	119
CDs/TiO_2	10 mL of 10 vol% methanol aqueous solution	350 W Xe lamp	250	N/A	120
CDs–NiP	40 mL of 10 vol% methanol aqueous solution	300 W Xe lamp (> 420)	40	1.4	124

QE: quantum efficiencies; PCN: polymeric carbon nitride; NPs: nanoparticles; N/A: not applicable; TEOA: triethanolamine; WC: tungsten carbide; CDs: carbon dots.

TiO_2-based photocatalysts are especially active for the H_2 evolution, presenting rates for the H_2 production of thousands of μmol g^{-1} h^{-1} with excellent quantum yields. However, it requires the use of UV irradiation, not being suitable for the harvesting of solar light.[31] As UV light only account for 4% of the total solar energy, even with 100% quantum efficiency the maximum theoretical STH is only 3.3%. This is less than the 5% required to meet the economic viability according to the U.S. Department of Energy (DOE).[19] In this context, TiO_2-based systems can become active under visible light irradiation via band-gap engineering or when combined with metal nanoparticles or other semiconductors. Nevertheless, these systems still present lower activities and quantum efficiencies when compared with to the best TiO_2-based under UV excitation. In this context, further TiO_2 hybridization strategies are required to improve activities under solar irradiation, and some strategies have shown promising results. This includes

Z-scheme approaches which may lead to good activities under visible light with relatively good quantum efficiency.

Another important class of photocatalysts are the CdS-based materials. These systems have shown the highest activities and quantum efficiencies under visible light.[91] On the other hand, they suffer from stability issues even when combined with other materials forming heterostructures. In this context, strategies where CdS is used as the core in core-shell structures have shown to be effective to increase CdS stability.[90] Nevertheless, the achieved stabilities are still lower than other commonly used photocatalysts (e.g., PCN and TiO_2) and still require the use of sacrificial reagents (S^{2-}/SO_3^{2-}).[15,90]

PCNs is another class of photocatalysts that is active under visible light irradiation while also being highly stable. Despite their remarkable stability, with PCN-based photocatalysts presenting no loss of efficiency even after 50 cycles (50 days),[19] they exhibit more modest activities and quantum efficiencies under visible light relative to CdS-based systems, due to their higher e^-/h^+ recombination rate.[47]

It is clear that the conversion of solar into chemical energy via the water splitting reaction, i.e., producing H_2 from water and sunlight, represents a remarkable and promising approach towards a sustainable future and meeting our growing energy demands. In this context, it is clear that several challenges must be overcome in terms of semiconductor photocatalyst design and performance in order to turn this vision into the reality. The semiconductor-based photocatalysts with the highest reproducible STH energy conversion reported are in the range of 1-2%.[19,126] As claimed by the U.S. Department of Energy (DOE), 5% is the minimum STH energy conversion that must be achieved to make the water splitting reaction economically feasible. Therefore, the ideal photocatalytic material requires high efficiency or performances under visible or near-infrared light excitation, high-stabilities, and compositions based on abundant (non-noble) components. In order to meet these design principles, progress in the areas of controlled synthesis, establishment of precise structure-performance relationships, advanced characterization, modelling, unravelling of photocatalytic enhancement mechanisms, and *in situ* and *in operando* characterization are crucial to enable a transition to a design driven approach, targeting better performances and stabilities. The development of new materials and morphologies and photocatalytic effects (such as localized surface plasmon resonance excitation) can also open new avenues for further exploitation and discovery to target performance goals towards the photocatalytic water splitting reaction.

Acknowledgments

This work was supported by FAPESP (grant 2015/26308-7), the Serrapilheira Institute (grant Serra-1709-16900), CNPq (grant 423196/2018-9), and start-up funds from University of Helsinki. J. Q., M. S. H., and I. F. T. thank FAPESP for the fellowships (grants 2016/17866-9, 2018/23495-9, and 2017/05506-0, respectively).

Ivo Teixeira *received his BSc in 2012 and his MSc in 2013 from the Federal University of Minas Gerais. He received his PhD from the University of Oxford in 2017, under the supervision of Prof Edman Tsang. After that, he joined Prof Pedro Camargo's group at University of São Paulo (Brazil) as a postdoctoral researcher and he has started his independent career as Professor at the Federal University of São Carlos (UFSCar) in 2019. His research interests include, but are not limited to, heterogeneous catalysis and photocatalysis applied for chemical synthesis, environmental remediation, and energy applications.*

Jhon Quiroz *received his BSc from the School of Chemistry at the Universidad Central de Venezuela in 2006. After getting his degree, he worked for three years as an assistant researcher in the Catalysis Division of the Venezuelan Petroleum Institute. In 2012, he obtained his Doctorate in Molecules and Condensed Matter at the Catalysis Unit and Solid State Chemistry Laboratory, University of Lille, in France. Currently, he works as a University Researcher at the University of Helsinki. His research focuses on the design and physicochemical characterization of plasmonic photocatalysts for more efficient conversion of solar to chemical energy.*

Mauricio Samuel Homsi *is an undergraduate student in Chemistry at University of São Paulo (Brazil) and Chemical Engineering undergraduate student at University Center of FEI (Brazil). His research interest includes photocatalysis and energy applications.*

Pedro Camargo *received his BSc and MSc in Chemistry in 2003 and 2005, respectively, from Federal University of Paraná in Brazil. He obtained his PhD in 2009 from Washington University in Saint Louis, working in Prof Younan Xia's group. In 2011, he was hired as an Assistant Professor at University of São Paulo. He was promoted to Associate Professor in 2015 and to Full Professor in 2018. In February of 2019, he relocated to a Professor position at the University of Helsinki. His research focuses on synthesis of nanomaterials for plasmonic nanocatalysis.*

References

1. Esswein, A. J.; Nocera, D. G.; *Chem. Rev.* **2007**, *107*, 4022.
2. Lewis, N. S.; Nocera, D. G.; *Proc. Natl. Acad. Sci. U. S. A.* **2006**, *103*, 15729.
3. Clark, W. C.; Dickson, N. M.; *Proc. Natl. Acad. Sci. U. S. A.* **2003**, *100*, 8059.
4. Bisquert, J.; *Nat. Photonics* **2008**, *2*, 648.
5. Ragauskas, A. J.; Williams, C. K.; Davison, B. H.; Britovsek, G.; Cairney, J.; Eckert, C. A.; Frederick Jr., W. J.; Hallett, J. P.; Leak, D. J.; Liotta, C. L.; Mielenz, J. R.; Murphy, R.; Templer, R.; Tschaplinski, T.; *Science* **2006**, *311*, 484.
6. Linic, S.; Christopher, P.; Ingram, D. B.; *Nat. Mater.* **2011**, *10*, 911.
7. Chen, C.; Ma, W.; Zhao, J.; *Chem. Soc. Rev.* **2010**, *39*, 4206.
8. Fujishima, A.; Honda, K.; *Nature* **1972**, *238*, 37.
9. Kato, H.; Asakura, K.; Kudo, A.; *J. Am. Chem. Soc.* **2003**, *125*, 3082.
10. Liu, G.; Wang, L.; Yang, H. G.; Cheng, H.-M.; Lu, G. Q. M.; *J. Mater. Chem.* **2010**, *20*, 831.
11. Hernández-Alonso, M. D.; Fresno, F.; Suárez, S.; Coronado, J. M.; *Energy Environ. Sci.* **2009**, *2*, 1231.
12. Tong, H.; Ouyang, S.; Bi, Y.; Umezawa, N.; Oshikiri, M.; Ye, J.; *Adv. Mater.* **2012**, *24*, 229.
13. Zhou, X.; Häublein, V.; Liu, N.; Nguyen, N. T.; Zolnhofer, E. M.; Tsuchiya, H.; Killian, M. S.; Meyer, K.; Frey, L.; Schmuki, P.; *Angew. Chem., Int. Ed.* **2016**, *55*, 3763.
14. Liu, N.; Häublein, V.; Zhou, X.; Venkatesan, U.; Hartmann, M.; Mackovic, M.; Nakajima, T.; Spiecker, E.; Osvet, A.; Frey, L.; *Nano Lett.* **2015**, *15*, 6815.
15. Chen, X.; Shen, S.; Guo, L.; Mao, S. S.; *Chem. Rev.* **2010**, *110*, 6503.
16. ASTM G173: *Standard Tables for Reference Solar Spectral Irradiances: Direct Normal and Hemispherical on 37° Tilted Surface*, West Conshohocken, 2012.
17. Peiris, S.; McMurtrie, J.; Zhu, H.-Y.; *Catal. Sci. Technol.* **2016**, *6*, 320.
18. Wang, Z.; Li, C.; Domen, K.; *Chem. Soc. Rev.* **2019**, *48*, 2109.
19. Liu, J.; Liu, Y.; Liu, N.; Han, Y.; Zhang, X.; Huang, H.; Lifshitz, Y.; Lee, S. T.; Zhong, J.; Kang, Z.; *Science* **2015**, *347*, 970.
20. Qureshi, M.; Takanabe, K.; *Chem. Mater.* **2016**, *29*, 158.
21. Chen, S.; Takata, T.; Domen, K.; *Nat. Rev. Mater.* **2017**, *2*, 17050.
22. Kudo, A.; Miseki, Y.; *Chem. Soc. Rev.* **2009**, *38*, 253.
23. Maeda, K.; *ACS Catal.* **2013**, *3*, 1486.
24. Wang, Y.; Suzuki, H.; Xie, J.; Tomita, O.; Martin, D. J.; Higashi, M.; Kong, D.; Abe, R.; Tang, J.; *Chem. Rev.* **2018**, *118*, 5201.
25. Moniz, S. J. A.; Shevlin, S. A.; Martin, D. J.; Guo, Z.-X.; Tang, J.; *Energy Environ. Sci.* **2015**, *8*, 731.
26. Hisatomi, T.; Kubota, J.; Domen, K.; *Chem. Soc. Rev.* **2014**, *43*, 7520.
27. Marschall, R.; *Adv. Funct. Mater.* **2014**, *24*, 2421.
28. Li, D.; Shi, J.; Li, C.; *Small* **2018**, *14*, 1704179.
29. Roger, I.; Shipman, M. A.; Symes, M. D.; *Nat. Rev. Chem.* **2017**, *1*, 0003.
30. Schrauzer, G. N.; Guth, T. D.; *J. Am. Chem. Soc.* **1977**, *99*, 7189.
31. Duonghong, D.; Borgarello, E.; Graetzel, M.; *J. Am. Chem. Soc.* **1981**, *103*, 4685.
32. Zhu, J.; Zäch, M.; *Curr. Opin. Colloid Interface Sci.* **2009**, *4*, 260.
33. Ahmad, H.; Kamarudin, S. K.; Minggu, L. J.; Kassim, M.; *Renewable Sustainable Energy Rev.* **2015**, *43*, 599.
34. Lu, X.; Wang, G.; Xie, S.; Shi, J.; Li, W.; Tong, Y.; Li, Y.; *Chem. Commun.* **2012**, *48*, 7717.
35. Kumar, S.; Kumar, A.; Rao, V. N.; Kumar, A.; Shankar, M. V.; Krishnan, V.; *ACS Appl. Energy Mater.* **2019**, *2*, 5622.
36. Kumar, S.; Reddy, N. L.; Kushwaha, H. S.; Kumar, A.; Shankar, M. V.; Bhattacharyya, K.; Halder, A.; Krishnan, V.; *ChemSusChem* **2017**, *10*, 3588.
37. Dong, H.; Li, J.; Chen, M.; Wang, H.; Jiang, X.; Xiao, Y.; Tian, B.; Zhang, X.; *Materials* **2019**, *12*, 2233.
38. Zhang, X.; Zhou, Y.-Z.; Wu, D.-Y.; Liu, X.-H.; Zhang, R.; Liu, H.; Dong, C.-K.; Yang, J.; Kulinich, S. A.; Du, X.-W.; *J. Mater. Chem. A* **2018**, *6*, 9057.
39. Kumar, S.; Reddy, N. L.; Kumar, A.; Shankar, M. V.; Krishnan, V.; *Int. J. Hydrogen Energy* **2018**, *43*, 3988.
40. Sayama, K.; Arakawa, H.; Domen, K.; *Catal. Today* **1996**, *28*, 175.
41. Domen, K.; Kudo, A.; Shinozaki, A.; Tanaka, A.; Maruya, K.-i.; Onishi, T.; *J. Chem. Soc., Chem. Commun.* **1986**, 356.
42. Kudo, A.; Tanaka, A.; Domen, K.; Maruya, K.-i.; Aika, K.-i.; Onishi, T.; *J. Catal.* **1988**, *111*, 67.
43. Buehler, N.; Meier, K.; Reber, J. F.; *J. Phys. Chem.* **1984**, *88*, 3261.
44. Chen, D.; Ye, J.; *J. Phys. Chem. Solids* **2007**, *68*, 2317.
45. Wu, C.-C.; Cho, H.-F.; Chang, W.-S.; Lee, T.-C.; *Chem. Eng. Sci.* **2010**, *65*, 141.
46. Maeda, K.; Wang, X.; Nishihara, Y.; Lu, D.; Antonietti, M.; Domen, K.; *J. Phys. Chem. C* **2009**, *113*, 4940.

47. Teixeira, I. F.; Barbosa, E. C. M.; Tsang, S. C. E.; Camargo, P. H. C.; *Chem. Soc. Rev.* **2018**, *47*, 7783.
48. Maeda, K.; Domen, K.; *J. Phys. Chem. C* **2007**, *111*, 7851.
49. Arai, N.; Saito, N.; Nishiyama, H.; Domen, K.; Kobayashi, H.; Sato, K.; Inoue, Y.; *Catal. Today* **2007**, *129*, 407.
50. Matsumura, M.; Saho, Y.; Tsubomura, H.; *J. Phys. Chem.* **1983**, *87*, 3807.
51. Reber, J. F.; Rusek, M.; *J. Phys. Chem.* **1986**, *90*, 824.
52. Darwent, J. R.; Mills, A.; *J. Chem. Soc., Faraday Trans. 2* **1982**, *78*, 359.
53. Erbs, W.; Desilvestro, J.; Borgarello, E.; Graetzel, M.; *J. Phys. Chem.* **1984**, *88*, 4001.
54. Ellis, A. B.; Kaiser, S. W.; Bolts, J. M.; Wrighton, M. S.; *J. Am. Chem. Soc.* **1977**, *99*, 2839.
55. Banin, U.; Ben-Shahar, Y.; Vinokurov, K.; *Chem. Mater.* **2013**, *26*, 97.
56. Waiskopf, N.; Ben-Shahar, Y.; Banin, U.; *Adv. Mater.* **2018**, *30*, 1706697.
57. Wang, H.; Zhang, L.; Chen, Z.; Hu, J.; Li, S.; Wang, Z.; Liu, J.; Wang, X.; *Chem. Soc. Rev.* **2014**, *43*, 5234.
58. Fu, J.; Yu, J.; Jiang, C.; Cheng, B.; *Adv. Energy Mater.* **2017**, *8*, 1701503.
59. Baffou, G.; Quidant, R.; *Chem. Soc. Rev.* **2014**, *43*, 3898.
60. Primo, A.; Corma, A.; García, H.; *Phys. Chem. Chem. Phys.* **2011**, *13*, 886.
61. Bamwenda, G. R.; Tsubota, S.; Nakamura, T.; Haruta, M.; *J. Photochem. Photobiol., A* **1995**, *89*, 177.
62. Primo, A.; Marino, T.; Corma, A.; Molinari, R.; Garcia, H.; *J. Am. Chem. Soc.* **2011**, *133*, 6930.
63. Li, K.; Zeng, Z.; Yan, L.; Luo, S.; Luo, X.; Huo, M.; Guo, Y.; *Appl. Catal., B* **2015**, *165*, 428.
64. Shiraishi, Y.; Kofuji, Y.; Kanazawa, S.; Sakamoto, H.; Ichikawa, S.; Tanaka, S.; Hirai, T.; *Chem. Commun.* **2014**, *50*, 15255.
65. Ong, W.-J.; Tan, L.-L.; Chai, S.-P.; Yong, S.-T.; *Dalton Trans.* **2015**, *44*, 1249.
66. Yu, J.; Wang, K.; Xiao, W.; Cheng, B.; *Phys. Chem. Chem. Phys.* **2014**, *16*, 11492.
67. Fina, F.; Menard, H.; Irvine, J. T. S.; *Phys. Chem. Chem. Phys.* **2015**, *17*, 13929.
68. Li, X.; Bi, W.; Zhang, L.; Tao, S.; Chu, W.; Zhang, Q.; Luo, Y.; Wu, C.; Xie, Y.; *Adv. Mater.* **2016**, *28*, 2427.
69. Jorge, A. B.; Martin, D. J.; Dhanoa, M. T. S.; Rahman, A. S.; Makwana, N.; Tang, J.; Sella, A.; Corà, F.; Firth, S.; Darr, J. A.; *J. Phys. Chem. C* **2013**, *117*, 7178.
70. Martin, D. J.; Qiu, K.; Shevlin, S. A.; Handoko, A. D.; Chen, X.; Guo, Z.; Tang, J.; *Angew. Chem., Int. Ed.* **2014**, *53*, 9240.
71. Wang, X.; Maeda, K.; Thomas, A.; Takanabe, K.; Xin, G.; Carlsson, J. M.; Domen, K.; Antonietti, M.; *Nat. Mater.* **2009**, *8*, 76.
72. Liu, J.; Zhang, Y.; Lu, L.; Wu, G.; Chen, W.; *Chem. Commun.* **2012**, *48*, 8826.
73. Tu, W.; Xu, Y.; Wang, J.; Zhang, B.; Zhou, T.; Yin, S.; Wu, S.; Li, C.; Huang, Y.; Zhou, Y.; Zou, Z.; Robertson, J.; Kraft, M.; Xu, R.; *ACS Sustainable Chem. Eng.* **2017**, *5*, 7260.
74. An, X.; Wang, W.; Wang, J.; Duan, H.; Shi, J.; Yu, X.; *Phys. Chem. Chem. Phys.* **2018**, *20*, 11405.
75. Zhang, Y.; Ligthart, D. A. J. M.; Quek, X.-Y.; Gao, L.; Hensen, E. J. M.; *Int. J. Hydrogen Energy* **2014**, *39*, 11537.
76. Chen, Y.; Lin, B.; Yu, W.; Yang, Y.; Bashir, S. M.; Wang, H.; Takanabe, K.; Idriss, H.; Basset, J.-M.; *Chem. - Eur. J.* **2015**, *21*, 10290.
77. Bi, L.; Xu, D.; Zhang, L.; Lin, Y.; Wang, D.; Xie, T.; *Phys. Chem. Chem. Phys.* **2015**, *17*, 29899.
78. Indra, A.; Menezes, P. W.; Kailasam, K.; Hollmann, D.; Schröder, M.; Thomas, A.; Brückner, A.; Driess, M.; *Chem. Commun.* **2016**, *52*, 104.
79. Zhang, G.; Huang, C.; Wang, X.; *Small* **2015**, *11*, 1215.
80. Sridharan, K.; Jang, E.; Park, J. H.; Kim, J. H.; Lee, J. H.; Park, T. J.; *Chem. - Eur. J.* **2015**, *21*, 9126.
81. Di, Y.; Wang, X.; Thomas, A.; Antonietti, M.; *ChemCatChem* **2010**, *2*, 834.
82. Guo, Y.; Jia, H.; Yang, J.; Yin, H.; Yang, Z.; Wang, J.; Yang, B.; *Phys. Chem. Chem. Phys.* **2018**, *20*, 22296.
83. Maeda, K.; Teramura, K.; Lu, D.; Takata, T.; Saito, N.; Inoue, Y.; Domen, K.; *Nature* **2006**, *440*, 295.
84. Majeed, I.; Manzoor, U.; Kanodarwala, F. K.; Nadeem, M. A.; Hussain, E.; Ali, H.; Badshah, A.; Stride, J. A.; Nadeem, M. A.; *Catal. Sci. Technol.* **2018**, *8*, 1183.
85. Brahimi, R.; Bessekhouad, Y.; Bouguelia, A.; Trari, M.; *J. Photochem. Photobiol., A* **2007**, *186*, 242.
86. Shen, S.; Guo, L.; Chen, X.; Ren, F.; Mao, S. S.; *Int. J. Hydrogen Energy* **2010**, *35*, 7110.
87. Hsieh, C.-T.; Chen, J.-M.; Lin, H.-H.; Shih, H.-C.; *Appl. Phys. Lett.* **2003**, *82*, 3316.
88. Chang, K.; Mei, Z.; Wang, T.; Kang, Q.; Ouyang, S.; Ye, J.; *ACS Nano* **2014**, *8*, 7078.
89. Jang, J. S.; Ham, D. J.; Lakshminarasimhan, N.; Choi, W. y.; Lee, J. S.; *Appl. Catal., A* **2008**, *346*, 149.
90. Xie, Y. P.; Yu, Z. B.; Liu, G.; Ma, X. L.; Cheng, H.-M.; *Energy Environ. Sci.* **2014**, *7*, 1895.
91. Yan, H.; Yang, J.; Ma, G.; Wu, G.; Zong, X.; Lei, Z.; Shi, J.; Li, C.; *J. Catal.* **2009**, *266*, 165.
92. Li, Y.; Chen, G.; Zhou, C.; Sun, J.; *Chem. Commun.* **2009**, 2020.
93. Li, Y.; Chen, G.; Wang, Q.; Wang, X.; Zhou, A.; Shen, Z.; *Adv. Funct. Mater.* **2010**, *20*, 3390.
94. Parida, K. M.; Martha, S.; Das, D. P.; Biswal, N.; *J. Mater. Chem.* **2010**, *20*, 7144.
95. Ding, X.; Li, Y.; Zhao, J.; Zhu, Y.; Li, Y.; Deng, W.; Wang, C.; *APL Mater.* **2015**, *3*, 104410.
96. Wen, J.; Xie, J.; Zhang, H.; Zhang, A.; Liu, Y.; Chen, X.; Li, X.; *ACS Appl. Mater. Interfaces* **2017**, *9*, 14031.

97. Ma, X.; Jiang, Q.; Guo, W.; Zheng, M.; Xu, W.; Ma, F.; Hou, B.; *RSC Adv.* **2016**, *6*, 28263.
98. Zhao, H.; Ding, X.; Zhang, B.; Li, Y.; Wang, C.; *Sci. Bull.* **2017**, *62*, 602.
99. Yin, W.; Bai, L.; Zhu, Y.; Zhong, S.; Zhao, L.; Li, Z.; Bai, S.; *ACS Appl. Mater. Interfaces* **2016**, *8*, 23133.
100. Lu, D.; Wang, H.; Zhao, X.; Kondamareddy, K. K.; Ding, J.; Li, C.; Fang, P.; *ACS Sustainable Chem. Eng.* **2017**, *5*, 1436.
101. Xu, Q.; Zhang, L.; Yu, J.; Wageh, S.; Al-Ghamdi, A. A.; Jaroniec, M.; *Mater. Today* **2018**, *5*, 1436.
102. Huang, D.; Chen, S.; Zeng, G.; Gong, X.; Zhou, C.; Cheng, M.; Xue, W.; Yan, X.; Li, J.; *Coord. Chem. Rev.* **2019**, *385*, 44.
103. Hu, J.; Wang, L.; Zhang, P.; Liang, C.; Shao, G.; *J. Power Sources* **2016**, *328*, 28.
104. Gao, H.; Zhang, P.; Hu, J.; Pan, J.; Fan, J.; Shao, G.; *Appl. Surf. Sci.* **2017**, *391*, 211.
105. Gao, H.; Zhang, P.; Zhao, J.; Zhang, Y.; Hu, J.; Shao, G.; *Appl. Catal., B* **2017**, *210*, 297.
106. Zhang, L. J.; Li, S.; Liu, B. K.; Wang, D. J.; Xie, T. F.; *ACS Catal.* **2014**, *4*, 3724.
107. Guo, H.-L.; Du, H.; Jiang, Y.-F.; Jiang, N.; Shen, C.-C.; Zhou, X.; Liu, Y.-N.; Xu, A.-W.; *J. Phys. Chem. C* **2017**, *121*, 107.
108. Wang, S.; Zhu, B.; Liu, M.; Zhang, L.; Yu, J.; Zhou, M.; *Appl. Catal., B* **2019**, *243*, 19.
109. Kailasam, K.; Fischer, A.; Zhang, G.; Zhang, J.; Schwarze, M.; Schröder, M.; Wang, X.; Schomäcker, R.; Thomas, A.; *ChemSusChem* **2015**, *8*, 1404.
110. Hou, H.; Gao, F.; Wang, L.; Shang, M.; Yang, Z.; Zheng, J.; Yang, W.; *J. Mater. Chem. A* **2016**, *4*, 6276.
111. Nowotny, M. K.; Sheppard, L. R.; Bak, T.; Nowotny, J.; *J. Phys. Chem. C* **2008**, *112*, 5275.
112. Gao, H.; Cao, R.; Xu, X.; Zhang, S.; Yongshun, H.; Yang, H.; Deng, X.; Li, J.; *Appl. Catal., B* **2019**, *245*, 399.
113. Jo, W.-K.; Selvam, N. C. S.; *Chem. Eng. J.* **2017**, *317*, 913.
114. Wang, Y.; Hu, A.; *J. Mater. Chem. C* **2014**, *2*, 6921.
115. Hu, C.; Li, M.; Qiu, J.; Sun, Y.-P.; *Chem. Soc. Rev.* **2019**, *48*, 2315.
116. Yu, H.; Shi, R.; Zhao, Y.; Waterhouse, G. I. N.; Wu, L. Z.; Tung, C. H.; Zhang, T.; *Adv. Mater.* **2016**, *28*, 9454.
117. Fernando, K. A. S.; Sahu, S.; Liu, Y.; Lewis, W. K.; Guliants, E. A.; Jafariyan, A.; Wang, P.; Bunker, C. E.; Sun, Y.-P.; *ACS Appl. Mater. Interfaces* **2015**, *7*, 8363.
118. Yu, H.; Zhao, Y.; Zhou, C.; Shang, L.; Peng, Y.; Cao, Y.; Wu, L.-Z.; Tung, C.-H.; Zhang, T.; *J. Mater. Chem. A* **2014**, *2*, 3344.
119. Wang, J.; Gao, M.; Ho, G. W.; *J. Mater. Chem. A* **2014**, *2*, 5703.
120. Wang, J.; Ng, Y. H.; Lim, Y.-F.; Ho, G. W.; *RSC Adv.* **2014**, *4*, 44117.
121. Fang, S.; Xia, Y.; Lv, K.; Li, Q.; Sun, J.; Li, M.; *Appl. Catal., B* **2016**, *185*, 225.
122. Wang, X.; Cheng, J.; Yu, H.; Yu, J.; *Dalton Trans.* **2017**, *46*, 6417.
123. Wang, Y.; Liu, X.; Liu, J.; Han, B.; Hu, X.; Yang, F.; Xu, Z.; Li, Y.; Jia, S.; Li, Z.; Zhao, Y.; *Angew. Chem., Int. Ed.* **2018**, *57*, 5765.
124. Martindale, B. C. M.; Hutton, G. A. M.; Caputo, C. A.; Reisner, E.; *J. Am. Chem. Soc.* **2015**, *137*, 6018.
125. Hutton, G. A. M.; Martindale, B. C. M.; Reisner, E.; *Chem. Soc. Rev.* **2017**, *46*, 6111.
126. Wang, Q.; Hisatomi, T.; Jia, Q.; Tokudome, H.; Zhong, M.; Wang, C.; Pan, Z.; Takata, T.; Nakabayashi, M.; Shibata, N.; *Nat. Mater.* **2016**, *15*, 611.

Submitted: August 18, 2019
Published online: November 7, 2019